Geosci. Model Dev. Discuss., 5, 119–148, 2012
www.geosci-model-dev-discuss.net/5/119/2012/
doi:10.5194/gmdd-5-119-2012

Geoscientific Model Development Discussions

Pre-industrial and mid-Pliocene simulations with NorESM-L

Z. S. Zhang[1,2,3], K. Nisancioglu[1,2], M. Bentsen[1,2], J. Tjiputra[1,2], I. Bethke[1,2], Q. Yan[3], B. Risebrobakken[1,2], C. Andersson[1,2], and E. Jansen[1,2]

[1]Bjerknes Centre for Climate Research, Allegaten 55, 5007, Bergen, Norway
[2]UNI Research, Allegaten 55, 5007, Bergen, Norway
[3]Nansen-Zhu International Research Center, Institute of Atmospheric Physics, Chinese Academy of Sciences, 100029, Beijing, China

Received: 20 December 2011 – Accepted: 10 January 2012 – Published: 13 January 2012

Correspondence to: Z. S. Zhang (zhongshi.zhang@bjerknes.uib.no)

Published by Copernicus Publications on behalf of the European Geosciences Union.

Abstract

The mid-Pliocene period (3.3 to 3.0 Ma) is known as a warm climate with atmospheric greenhouse gas levels similar to the present. As the climate at this time was in equilibrium with the greenhouse forcing, it is a valuable test case to better understand the long term response to high levels of atmospheric greenhouse gases. In this study, we use the low resolution version of the Norwegian Earth System Model (NorESM-L) to simulate the pre-industrial and the mid-Pliocene climate. Comparison of the simulation with observations demonstrates that NorESM-L simulates a realistic pre-industrial climate. The simulated mid-Pliocene global mean surface air temperature is 16.7 °C, which is 3.2 °C warmer than the pre-industrial. The simulated mid-Pliocene global mean sea surface temperature is 19.1 °C, which is 2.0 °C warmer than the pre-industrial. The warming is relatively uniform globally, except for a strong amplification at high latitudes.

1 Introduction

The mid-Pliocene period, also referred to as the mid-Piacenzian, is known as the most recent period in Earth's history when the global average temperature was warmer than today. Estimates are on the order of 2–3 °C warmer compared to today (Jansen et al., 2007; Dowsett et al., 2010). This warming is accompanied by global sea level that was 10–45 m higher than present (e.g. Raymo et al., 1996). The warming is within the range of the Intergovernmental Panel on Climate Change (IPCC) projections of global temperature increases for the 21st century (Meehl et al., 2007). Unlike other warm geological periods, e.g. Eocene and Miocene, the paleogeography of the mid-Pliocene is similar to the present. Thus, the mid-Pliocene climate has been considered as an analog for the long term fate of the climate system under the present level of greenhouse gases forcing.

The mid-Pliocene has been a focus for several data synthesis (e.g. Dowsett et al., 1994, 1996, 1999, 2009, 2010) and modeling (e.g. Chandler et al., 1994; Sloan et al.,

1996; Haywood et al., 2000; Haywood and Valdes, 2004; Jiang et al., 2005; Yan et al., 2011). However, early model studies indicated a clear model-data discrepancy. Interpretation of the proxy data suggested that the Atlantic Meridional Overturning Circulation (AMOC) was stronger in the mid-Pliocene compared to the present (Raymo et al., 1996; Ravelo et al., 2000; Hodell et al., 2006). The enhanced AMOC was thought to have lead to increased northward heat transport and warm temperatures in the high latitude Atlantic and Arctic (Dowsett el al., 1992; Dowsett et al., 2009). However, most climate models forced with mid-Pliocene boundary conditions did not simulate a stronger AMOC and enhanced heat transport (e.g. Haywood and Valdes, 2004; Yan et al., 2011). Thus, to better understand the dynamics behind the estimated high latitude warmth of the mid-Pliocene, and to assess the ability of climate models in simulating a past warm climate, the Pliocene Paleoclimate Modeling Intercomparison Project (PlioMIP) was recently initiated (Haywood et al., 2010, 2011).

The pre-industrial and mid-Pliocene experiments with the low resolution version of the Norwegian Earth System Model (NorESM-L) presented in this paper is a contribution from t the Bjerknes Centre for Climate Research (BCCR) and the Norwegian Climate Centre (NCC) to the PlioMIP experiment II. The NorESM-L model is introduced in detail in Sect. 2. Section 3 describes the experimental design, and Sect. 4 discusses the results. A brief discussion and summary are given in Sect. 5.

2 Model description

The NorESM is an earth system model built under the structure of the Community Earth System Model (CESM) from the National Center for Atmospheric Research (NCAR). It uses the same coupler (CLP7), atmosphere (CAM4), land (CLM4), and sea ice (CICE4) components as the CESM. The key difference to the standard CESM configuration is an optional modification to the treatment of atmospheric chemistry, aerosols, and clouds (Seland et al., 2008) and the ocean component that is the Miami Isopycnic Coordinate

Ocean Model (MICOM) in the NorESM. Simulations with the NorESM are the contributions from the Norwegian Climate Centre (NCC) to the Coupled Model Intercomparison Project Phase 5 (CMIP5), which is expected to be included in the upcoming Intergovernmental Panel on Climate Change (IPCC) Fifth Assessment Report (AR5).

In this study we use the low resolution version of the NorESM (NorESM-L). The horizontal resolution for the atmosphere is T31, with 26 levels in the vertical. This corresponds roughly to a grid size of approximately 3.75 degrees. The horizontal resolution in the ocean is g37, corresponding to a nominal grid size of 3 degrees. The ocean component has 30 isopycnic layers in the vertical. Detailed documentations for each component of the model system are given in the following sections.

2.1 Atmospheric model

The atmosphere component of the NorESM-L is the spectral Community Atmosphere Model CAM4 (Neale et al., 2010; Eaton, 2010). It uses the Eulerian dynamical core, which is based on the hybrid vertical coordinate developed by Simmons and Strüfing (1981). The model includes physical parameterizations of convection, clouds, surface processes, and turbulent mixing. The parameterization of deep convection uses the scheme developed by Zhang and McFarlane (1995), together with the convective momentum transport modification developed by Richter and Rasch (2008), and the dilute plume modification developed by Raymond and Blyth (1986, 1992). The parameterization of clouds uses the scheme introduced by Slingo (1987), with the variations described in Hack et al. (1993), Kiehl et al. (1998), and Rasch and Kristjánsson (1998). The parameterization of surface processes uses a bulk exchange formulation described in Neal et al. (2010) to calculate the surface exchange of heat, moisture and momentum between the atmosphere and land, ocean or ice surfaces. The parameterization of turbulence includes the scheme of free atmosphere turbulent diffusivities and the scheme of non-local atmospheric boundary layer parameterization described in Holtslag and Boville (1993) and Neale et al. (2010). The standard CAM4

treatment of atmospheric chemistry, aerosols, and clouds is used in this study. Detailed introduction to CAM4 can be found in the scientific description of CAM4 (Neale et al., 2010) and the user guide (Eaton, 2010).

2.2 Land model

The land component used in NorESM-L is the Community Land Model CLM4 (Oleson et al., 2010; Kluzek, 2011). It calculates radiation and heat fluxes at the land-atmosphere interface, as well as temperature, humidity, and soil thermal and hydrologic states. The sub-grid scale surface heterogeneity is represented through fractional coverage of glacier, lake, wetland, urban, and vegetation consisting of up to 15 plant functional types (PFTs) plus bare ground. Soil colors in the model are fitted to a range of 20 soil classes. The radiation fluxes are calculated according to the formulation introduced in Oleson et al. (2010). The heat fluxes are calculated using the Monin-Obukhov similarity theory as described in Zeng et al. (1998). Soil and snow temperatures are calculated according to the numerical solution introduced in Oleson et al. (2010). The model calculates changes in canopy water, snow water, soil water, and soil ice and water. A river transport model is included to give a closed hydrological cycle. Detailed descriptions of CLM4 can be found in the technical description (Oleson et al., 2010) and the user guide (Kluzek, 2011).

2.3 Sea ice model

The sea ice component used in NorESM-L is the Community Ice CodE CICE4 (Bailey et al., 2010; Hunke and Lipscomb, 2010). In the CICE model, the evolution of ice thickness distribution is controlled by the three types of sea ice transport, including transport in horizontal space following an incremental remapping scheme (Dukowicz and Baumgardner, 2000; Lipscomb and Hunke, 2005), transport in thickness space due to thermodynamic growth following the Lipscomb remapping scheme (Lipscomb, 2001), and the melting and redistribution of ice in thickness space due to ridging and other

mechanical processes (Thorndike et al., 1975; Rothrock, 1975; Hibler, 1980; Flato and Hibler, 1995; Lipcomb et al., 2007). Elastic-viscous-plastic ice dynamics (Hunke and Dukowicz, 1997) are used to calculated velocity. The Bitz-Lipscomb thermodynamic model (Bitz and Lipscomb, 1999) is employed to compute ice growth rate. Detailed introduction to CICE can be found in the CICE documentation and user manual (Hunke and Lipscomb, 2010) and the user guide (Bailey et al., 2010).

2.4 Ocean model

The ocean component used in the NorESM-L is founded on the Miami Isopycnic Coordinate Ocean Model MICOM (Bleck and Smith, 1990; Bleck et al., 1992), which uses potential density as vertical coordinate. The model consists of a stack of 30 isopycnal layers evaluated with a reference pressure of 2000 db, and a mixed layer on top represented by two non-isopycnal layers, providing the linkage between the atmospheric forcing and the ocean interior. Modifications of the original MICOM have been prompted by the desire to improve conservation of mass, heat, and tracers and to implement robust, accurate, and efficient transport of many tracers that is particular important for ocean biogeochemistry modeling. Further, the pressure gradient force is now accurately estimated using in situ density, the diapycnal diffusion equation is solved by an implicit method, and numerous physical parameterizations have been improved or added in order to reduce model biases particular in coupled climate model configurations. These changes are described in Assmann et al. (2010) and Alterskjær et al. (2011).

3 Experimental designs

3.1 Pre-industrial control experiment

Following the PlioMIP experimental guidelines (Haywood et al., 2011), the pre-industrial control experiment presented in this paper uses the modern land-sea mask,

topography, ice-sheets and vegetation. All these geographic boundary conditions are taken from the CESM (Vertenstein et al., 2011). The ocean model uses the modern bathymetry and is initialized from Levitus temperature and salinity (Levitus and Boyer, 1994). Atmospheric greenhouse gases are set to the pre-industrial values of 280 ppm CO_2, 270 ppb N_2O, 760 ppb CH_4, and zero levels of CFCs. Solar constant are set to 1370 W m^{-2}. Orbital parameters are set to the values for 1950 (Berger, 1978). The pre-industrial aerosols conditions from the CESM (Vertenstein et al., 2011) are used in the pre-industrial control experiment. With these boundary conditions and initial conditions, the pre-industrial control experiment is run for 1500 yr.

3.2 Mid-Pliocene experiment

In the mid-Pliocene experiment, the conditions for the ocean model are set following the PlioMIP experiment guidelines (Haywood et al., 2011). The land-sea mask and bathymetry in the mid-Pliocene experiment are the same as those in the pre-industrial experiment. The Central American Seaway (Panama Gateway) is kept closed, and the Bering Strait, Madagascar Strait, Drake Passage, Tasman Gateway, Gibraltar Strait and Indonesian Gateway are kept opened. The PRSIM DOT deep ocean temperature (Dowsett et al., 2009) is not used to initialize the ocean model in the mid-Pliocene experiment. Instead, initial temperature and salinity from Levitus and Boyer (1994) are used in the mid-Pliocene experiment. This is the same as that used in the pre-industrial control run.

The PRISM Pliocene topography file topo_v1.3 (Sohl et al., 2009) is used to build the topography for the experiment. The difference between PRISM Pliocene topography and PRISM modern topography is interpolated to the T31 resolution. Then, the interpolated difference is added to the modern topography used in the pre-industrial experiment.

The PRISM Pliocene vegetation biom_veg_v1.2 (Hill et al., 2007; Salzmann et al., 2008) is used to construct the vegetation and ice-sheets for the mid-Pliocene experiment. The PRISM Pliocene vegetation is interpolated to the T31 resolution.

Subsequently, the biome vegetation types are changed to the LSM vegetation types, according to the table named Biome4 conversion to LSM edited by Rosenbloom (2009). Finally, the LSM vegetation file is converted to appropriate boundary conditions for the CLM using the CCSM paleoclimate tools from NCAR (Rosenbloom et al., 2010).

For the greenhouse gases, the atmospheric CO_2 level is set to 405 ppm. Other greenhouse gases are kept at the same levels as those in the pre-industrial control experiment. Other boundary conditions, including solar constant, orbital parameters and aerosols, are also kept at the same as those used in the pre-industrial control run.

3.3 Time integration

The pre-industrial and mid-Pliocene experiments are both run for 1500 yr. Time series of the top of the atmosphere energy balance, global mean surface air temperature and maximum Atlantic Meridional Overturning Circulation (AMOC) are shown in Fig. 1. Both experiments reach an equilibrium state after approximately 1000 yr of model integration time. In this paper we calculate the climatological means from the last 200 yr of each simulation.

4 Results

4.1 Pre-industrial control experiment

4.1.1 Surface air temperature

For the pre-industrial experiment, global annual mean surface air temperature (SAT) is 13.5 °C (Fig. 1), in good agreement with pre-industrial temperature estimates (e.g. Hansen et al., 2010). The zonal mean SAT (Fig. 2a) shows that the annual mean temperature at the North Pole is about −20 °C, whereas it is −44 °C close to the South Pole. The warmest temperatures are found over the western tropical Pacific and eastern tropical Indian Ocean, with temperatures higher than 28 °C (Fig. 3a). The coldest

temperatures are found over East Antarctica with temperatures below −50 °C. The zero degree isotherm in the Southern Hemisphere is relatively zonal and located close to 60 °S. In contrast, the zero degree isotherm in the Northern Hemisphere is strongly influenced by topography and land-sea distribution. It is located close to 70° N over the Labrador Sea and the Norwegian Sea, and close to 60° N in the North Pacific.

The simulated pre-industrial SAT is in good agreement with the ERA-interim (Dee et al., 2011) temperature data (Fig. 3b). However, as expected, the simulated pre-industrial temperatures are slightly colder than the modern estimates represented by the ERA-interim data.

4.1.2 Precipitation

In the pre-industrial experiment, the global annual mean precipitation is 2.7 mm day^{-1}, with a peak in annual zonal mean precipitation in the Intertropical Convergence Zone (ITCZ) of about 6.5 mm day^{-1} (Fig. 2b). The lowest precipitation, about 0.2 mm day^{-1}, appears close to the South Pole. Regionally (Fig. 3c), high precipitation can be seen over the tropical ocean and continent, with annual mean precipitation higher than 12 mm day^{-1} over the western tropical Pacific. In the Sahara and over East Antarctica, precipitation is less than 0.2 mm day^{-1}.

Compared to the observed precipitation data from the Global Precipitation Climatology Project (GPCP; Adler et al., 2003) averaged over the period 1979–2008 (Fig. 3d), the overall pattern and amount are in good agreement. However model-data discrepancies exist in the tropics and in the Southern Hemisphere sub-tropical oceans, where the simulated precipitation is larger than the observations.

4.1.3 Sea surface temperature

In the pre-industrial experiment, the global annual mean SST is 17.1°C, with the warmest temperatures, larger than 28 °C, in the western tropical Pacific and eastern tropical Indian Ocean (Fig. 4a). The zero degree isotherm is located close to 60 °S

in the Southern Hemisphere, and around the margin of Arctic in the Northern Hemisphere.

The simulated SSTs compare well with the data of Levitus and Boyer (1994) (Fig. 4b). However, the model simulations are slightly cooler than the observations, in particular in the tropical oceans. This is expected as the observations represent today's SST and not pre-industrial values.

4.1.4 Sea surface salinity

High sea surface salinity occurs generally at the surface of the subtropical oceans (Fig. 4c). Salinity is relatively low at the surface of the tropical and high latitude oceans. The highest salinities, close to 38 g kg^{-1}, appear at the surface of the Mediterranean Sea. The lowest salinities, with salinity less than 32 g kg^{-1}, occur at the surface of marginal seas in the Arctic, the Hudson Bay (northeastern North American), the Gulf of Guinea (eastern tropical Atlantic) and the Indonesian archipelago (western tropical Pacific).

The global sea surface pattern (Fig. 4d) agrees well with observations (Levitus and Boyer, 1994). However, simulated salinities are a little lower than observed values at the surface of the Atlantic Ocean, but higher in the Arctic and the North Pacific.

4.2 Mid-Pliocene experiment

4.2.1 Surface temperature

In the mid-Pliocene experiment, the global annual mean SAT is 16.7 °C (Fig. 1). The zonal mean annual SAT shows that the annual mean temperature close to the South Pole is about −40 °C, whereas it is about 7 °C close to the North Pole (Fig. 2a). The annual mean temperature is about 27 °C at the equator.

Compared to the pre-industrial control run, the simulated mid-Pliocene global annual mean SAT is 3.2 °C warmer. Warming occurs almost globally (Fig. 5a), with stronger

warming appearing in high latitudes. Cooler temperatures are simulated over parts of the western tropical Pacific, the Southern Ocean close to West Antarctica, tropical Africa, East Australia, and East Antarctica.

The warming can also be seen in the seasonal SAT anomalies between the mid-Pliocene and the pre-industrial. In boreal summer (Fig. 5b), the warming exceeds 5 °C over Greenland in the Northern Hemisphere, and around the margin of Antarctica in the Southern Hemisphere. In boreal winter (Fig. 5c), the middle and high latitude continents are significantly warmer in the Northern Hemisphere, with a temperature increase at the mid-Pliocene of more than 5 °C. The warming increases northward towards the North Pole, where temperatures increase as much as 20 °C. In the Southern Hemisphere, the strongest warming occurs around the Antarctic margin with temperatures increasing more than 5 °C.

4.2.2 Precipitation

In the mid-Pliocene experiment, the global annual mean precipitation is 2.9 mm day^{-1}. The zonal mean annual precipitation shows that largest precipitation appears near the equator, with about 7.3 mm day^{-1} (Fig. 2b). The lowest precipitation, about 0.2 mm day^{-1}, appears close to the South Pole.

Compared to the pre-industrial experiment, the simulated mid-Pliocene global annual mean precipitation increases by about 0.2 mm day^{-1}. Precipitation increases in the tropics north of the equator by 1 mm day^{-1}, and in the middle and high latitudes of both hemispheres by 0.5 mm day^{-1}. Precipitation decreases in the subtropics of the Northern Hemisphere by 0.1 mm day^{-1}, and tropics of the Southern Hemisphere (Fig. 6a) by 0.9 mm day^{-1}. The differences similar to those of the zonal mean annual precipitation are also simulated in the seasonal precipitation anomalies (Fig. 6b, c).

4.2.3 Sea surface temperature

In the mid-Pliocene experiment (Fig. 7a), the warmest ocean surfaces with temperature higher than 28°C appear in the tropical Indian Ocean, the western tropical Pacific, the eastern tropical Pacific and the eastern tropical Atlantic. The zero degree isotherm almost disappears in the Southern Hemisphere. In the Northern Hemisphere, it is located further north than in the pre-industrial, and at about 75° N in the Arctic Ocean.

Compared to the pre-industrial SST, almost the entire ocean surface is warmer in the mid-Pliocene experiment (Fig. 7b). The strongest warming, with SST increased by more than 3 °C, occurs at the surface of the Greenland Sea, the central North Atlantic, the Japanese Sea and the Southern Ocean off East Antarctica. There are only a few small regions where temperatures decrease (by less than 1 °C) in the mid-Pliocene relative to the pre-industrial experiment. These regions can be found in the Norwegian Sea, the Labrador Sea, the western tropical Pacific, and the Southern Ocean off the coast of west Antarctica.

4.2.4 Sea surface salinity

The basic pattern of mid-Pliocene SSS is similar as the pre-industrial (Fig. 7c). However, the mid-Pliocene salinity decreases at the surface of the Arctic and the Indian Ocean relative to the pre-industrial by 2 g kg^{-1} (Fig. 7d), but increases at the surface of the Atlantic, the Pacific, and the Southern Ocean by 1 g kg^{-1}. Large SSS increases ($\Delta SSS > 0.6$ g kg^{-1}) appear in the central North Atlantic, the Mediterranean Sea, the western tropical Pacific, the western coast of central America, the tropical Atlantic, and the Southern Ocean off East Antarctica.

5 Discussion

As described in the previous section, the NorESM-L pre-industrial simulation is in good agreement with observations. The simulated mid-Pliocene climate is warmer,

as expected due to the elevated atmospheric CO_2 level. Most of this warming is concentrated at high latitudes, and is most pronounced in the Arctic during boreal winter. The simulated high latitude warmth is consistent with the PRISM sea surface temperature reconstructions (Dowsett et al., 2009, 2010), although the proxy set is very sparse in the Nordic Seas and Arctic.

Earlier studies have pointed to an enhanced AMOC to account for reconstructions of relatively warm mid-Pliocene sea surface temperatures in the North Atlantic (Dowsett el al., 1992; Raymo et al., 1996; Ravelo et al., 2000; Hodell et al., 2006; Dowsett et al., 2009, 2010). However, in our study the simulated AMOC is similar to that of the pre-industrial, with a maximum overturning stream function only 1.6 Sv stronger in the mid-Pliocene. More importantly, the return flow of NADW occurs at a slightly shallower depth in the mid-Pliocene experiment (Fig. 8).

Although the AMOC is slightly stronger in the mid-Pliocene experiment, the total northward heat transport by the Atlantic is reduced (not shown). Thus, the simulated warm surface temperatures at high latitudes of the North Atlantic cannot be attributed to changes in ocean overturning or ocean heat transport. A more likely candidate for the surface warming is the reduced size of the Greenland ice sheet (Lunt et al., 2009). Other possible mechanisms are (1) a reduction in sea ice, (2) increased poleward atmospheric heat transport, (3) strong near-surface atmospheric stability leading to a large, albeit shallow high-latitude temperature response and (4) enhanced downward long-wave radiation due to changes in atmospheric moisture and clouds. However, a detailed investigation of these mechanisms is beyond the scope of this paper, and will be pursued in a future publication.

6 Summary

In this paper, we describe pre-industrial and mid-Pliocene experiments simulated with the NorESM-L. Comparison of the simulation with observations demonstrates that the NorESM-L simulates a realistic pre-industrial climate. Compared to the pre-industrial

simulation, the global mid-Pliocene surface temperature is 3.2 °C warmer. Warming occurres almost globally, with stronger warming occuring in the high latitudes. In the mid-Pliocene experiment, global annual mean precipitation increases by 0.2 mm day^{-1}.

At the ocean surface, the simulated mid-Pliocene global mean SST is 2.0 °C warmer than the pre-industrial. More importantly, the warming exceeds 3 °C at the surface of the Greenland Sea, in the central North Atlantic, and in the Southern Ocean off the coast of East Antarctica. Salinity increases at the surface of the Atlantic, the Pacific and the Southern Ocean by 1 g kg^{-1}, but decreases at the surface of the Arctic and the Indian oceans by 2 g kg^{-1}.

Acknowledgements. This study was jointly supported by the Earth System Modeling (ESM) project financed by Statoil, Norway, the National 973 Program of China (Grant No. 2010CB950102), and the National Natural Science Foundation of China (Grant No. 40902054). The NorESM development was supported by the Integrated Earth System Approach to Explore Natural Variability and Climate Sensitivity (EARTHCLIM) project, which is a nationally coordinated climate research project in Norway.

References

Adler, R. F., Huffman, G. J., Chang, A., Ferraro, R., Xie, P., Janowiak, J., Rudolf, B., Schneider, U., Curtis, S., Bolvin, D., Gruber, A., Susskind, J., and Arkin, P.: The Version 2 Global Precipitation Climatology Project (GPCP) Monthly Precipitation Analysis (1979–Present), J. Hydrometeor., 4, 1147–1167, 2003.

Alterskjær, K., Kristjánsson, J. E., and Seland, Ø.: Sensitivity to deliberate sea salt seeding of marine clouds – observations and model simulations, Atmos. Chem. Phys. Discuss., 11, 29527–29559, doi:10.5194/acpd-11-29527-2011, 2011.

Assmann, K. M., Bentsen, M., Segschneider, J., and Heinze, C.: An isopycnic ocean carbon cycle model, Geosci. Model Dev., 3, 143–167, doi:10.5194/gmd-3-143-2010, 2010.

Bailey, D., Holland, M., Hunke, E., Lipscomb, B., Briegleb, B., Bitz, C., and Schramm, J.: Community Ice CodE (CICE) User's Guide Version 4.0, available at: http://www.cesm.ucar.edu/models/cesm1.0/cice/doc/index.html (last access: December 2011), 2010.

Berger, A.: Long Term Variations of Daily Insolation and Quaternary Climatic Changes, J. Atmos. Sci., 35, 2362–2367, 1978.

Bitz, C. M. and Lipscomb, W. H.: An energy-conserving thermodynamic sea ice model for climate study, J. Geophys. Res.-Oceans, 104, 15669–15677, 1999.

Bleck, R. and Smith, L. T.: A Wind-Driven Isopycnic Coordinate Model of the North and Equatorial Atlantic Ocean, 1. Model Development and Supporting Experiments, J. Geophys. Res., 95, 3273–3285, 1990.

Bleck, R., Rooth, C., Hu, D., and Smith, L. T.: Salinity-driven Thermocline Transients in a Wind- and Thermohaline-forced Isopycnic Coordinate Model of the North Atlantic, J. Phys. Oceanogr., 22, 1486–1505, 1992.

Chandler, M., Rind, D., and Thompson, R.: Joint investigations of the middle Pliocene climate II: GISS GCM Northern Hemisphere results, Global Planet. Change, 9, 197–219, 1994.

Dee, D. P., Uppala, S. M., Simmons, A. J., Berrisford, P., Poli, P., Kobayashi, S., Andrae, U., Balmaseda, M. A., Balsamo, G., Bauer, P., Bechtold, P., Beljaars, A. C. M., van de Berg, L., Bidlot, J., Bormann, N., Delsol, C., Dragani, R., Fuentes, M., Geer, A.J., Haimberger, L., Healy, S.B., Hersbach, H., Hólm, E. V., Isaksen, L., Kållberg, P., Köhler, M., Matricardi, M., McNally, A. P., Monge-Sanz, B.M., Morcrette, J. J., Park, B. K., Peubey, C., de Rosnay, P., Tavolato, C., Thépaut, J. N., Vitart, F.: The ERA-Interim reanalysis: configuration and performance of the data assimilation system, Quart. J. Roy. Meteorol. Soc., 137, 553–597, doi:10.1002/qj.828, 2011.

Dowsett, H. J., Barron, J., and Poore, R.: Middle Pliocene sea surface temperatures: a global reconstruction, Mar. Micropaleontol., 27, 13–25, 1996.

Dowsett, H. J., Barron, J. A., Poore, R. Z., Thompson, R. S., Cronin, T. M., Ishman, S. E., and Willard, D. A.: Middle Pliocene paleoenvironmental reconstruction: PRISM2, US Geol. Surv., Open File Rep., 99–535, 1999.

Dowsett, H. J., Robinson, M. M., and Foley, K. M.: Pliocene three-dimensional global ocean temperature reconstruction, Clim. Past, 5, 769–783, doi:10.5194/cp-5-769-2009, 2009.

Dowsett, H. J., Robinson, M. M., Haywood, A. M., Salzmann, U., Hill, D., Sohl, L., Chandler, M., Williams, M., Foley, K., and Stoll, D.: The PRISM3D paleoenvironmental reconstruction, Stratigraphy, 7, 123–139, 2010.

Dowsett, H. J., Thompson, R., Barron, J., Cronin, T., Fleming, F., Ishman, S., Poore, R.,Willard, D., and Holtz, T.: Joint Investigations of the Middle Pliocene Climate I: PRISM Paleoenvironmental Reconstructions, Global Planet. Change, 9, 169–195, 1994.

Dowsett, H. J., Cronin, T. M., Poore, R. Z., Thompson, R. S., Whatley, R. C., and Wood, A. M.: Micropaleontological evidence for increased meridional heat transport in the North Atlantic Ocean during the Pliocene, Science, 258, 1133–1135, 1992.

Dukowicz, J. K. and Baumgardner, J. R.: Incremental remapping as a transport/advection algorithm, J. Comput. Phys., 160, 318–335, 2000.

Eaton, B.: User's Guide to the Community Atmosphere Model CAM-4.0, available at: http://www.cesm.ucar.edu/models/ccsm4.0/cam/docs/users_guide/ug.html (last access: December 2011), 2010.

Flato, G. M. and Hibler, W. D.: Ridging and strength in modeling the thickness distribution of Arctic sea ice, J. Geophys. Res.-Oceans, 100, 18611–18626, 1995.

Hack, J. J., Boville, B. A., Briegleb, B. P., Kiehl, J. T., Rasch, P. J., and Williamson, D. L.: Description of the NCAR Community Climate Model (CCM2), Technical Report NCAR/TN-382+STR, National Center for Atmospheric Research, 120 pp., 1993.

Hansen, J., Ruedy, R., Sato, M., and Lo, K.: Global surface temperature change, Rev. Geophys., 48, RG4004, doi:10.1029/2010RG000345, 2010.

Haywood, A. M. and Valdes, P. J.: Modelling Pliocene warmth: contribution of atmosphere, oceans and cryosphere, Earth Planet. Sci. Lett., 218, 363–377, 2004.

Haywood, A. M., Valdes, P. J., and Sellwood, B. W.: Global scale palaeoclimate reconstruction of the middle Pliocene climate using the UKMO GCM: initial results, Global Planet. Change, 25, 239–256, 2000.

Haywood, A. M., Dowsett, H. J., Otto-Bliesner, B., Chandler, M. A., Dolan, A. M., Hill, D. J., Lunt, D. J., Robinson, M. M., Rosenbloom, N., Salzmann, U., and Sohl, L. E.: Pliocene Model Intercomparison Project (PlioMIP): experimental design and boundary conditions (Experiment 1), Geosci. Model Dev., 3, 227–242, doi:10.5194/gmd-3-227-2010, 2010.

Haywood, A. M., Dowsett, H. J., Robinson, M. M., Stoll, D. K., Dolan, A. M., Lunt, D. J., Otto-Bliesner, B., and Chandler, M. A.: Pliocene Model Intercomparison Project (PlioMIP): experimental design and boundary conditions (Experiment 2), Geosci. Model Dev., 4, 571–577, doi:10.5194/gmd-4-571-2011, 2011.

Hibler, W. D.: Modeling a variable thickness sea ice cover, Mon. Weather Rev., 108, 1943–1973, 1980.

Hill, D. J., Haywood, A. M., Hindmarsh, R. C. A., and Valdes, P. J.: Characterising ice sheets during the mid Pliocene: evidence from data and models, in: Deep time perspectives on climate change: Marrying the signal from computer models and biological proxies, edited by:

Williams, M., Haywood, A. M., Gregory, F. J., and Schmidt, D. N., the Micropalaeontological Society, Special Publications, the Geological Society, London, 517–538, 2007.
Hodell, D. A. and Venz-Curtis, K. A.: Late Neogene history of deepwater ventilation in the southern ocean, Geochem. Geophys. Geosyst., 7, Q09001, doi:10.1029/2005GC001211, 2006.
Holtslag, A. A. M. and Boville, B. A.: Local versus nonlocal boundary-layer diffusion in a global climate model, J. Climate, 6, 1825–1842, 1993.
Hunke, E. C. and Dukowicz, J. K.: An elastic-viscous-plastic model for sea ice dynamics, J. Phys. Oceanogr., 27, 1849–1867, 1997.
Hunke, E. C. and Lipscomb, W. H.: CICE: the Los Alamos Sea Ice Model Documentation and Software User's Manual Version 4.1, LA-CC-06-012, available at: http://oceans11.lanl.gov/trac/CICE (last access: December 2011), 2010.
Jansen, E., Overpeck, J., Briffa, K. R., Duplessy, J.-C., Joos, F., Masson-Delmotte, V., Olago, D., Otto-Bliesner, B., Peltier, W. R., Rahmstorf, S., Ramesh, R., Raynaud, D., Rind, D., Solomina, O., Villalba, R., and Zhang, D.: Palaeoclimate, in: Climate Change 2007: The Physical Science Basis. Contribution of Working Group I to the Fourth Assessment Report of the Intergovernmental Panel on Climate Change, edited by: Solomon, S., Qin, D., Manning, M., Chen, Z., Marquis, M., Averyt, K. B., Tignor, M., and Miller, H. L., Cambridge University Press, Cambridge, United Kingdom and New York, NY, USA, 2007.
Jiang, D., Wang, H., Ding, Z., Lang, X., and Drange, H.: Modeling the middle Pliocene climate with a global atmospheric general circulation model, J. Geophys. Res., 110, D14107, doi:10.1029/2004JD005639, 2005.
Kiehl, J. T., Hack, J. J., Bonan, G. B., Boville, B. B., Williamson, D. L., and Rasch, P. J.: The National Center for Atmospheric Research Community Climate Model: CCM3, J. Climate, 11, 1131–1149, 1998.
Kluzek, E.: CESM Research Tools: CLM4 in CESM1.0.3 user's guide documentation, available at: http://www.cesm.ucar.edu/models/cesm1.0/clm/models/lnd/clm/doc/UsersGuide/book1.html (last access: December 2011), 2011.
Levitus, S. and Boyer, T. P.: World Ocean Atlas Volume 4: Temperature, NOAA Atlas NESDIS 4, US Government Printing Office, Washington, DC, 117, 1994.
Lipscomb, W. H.: Remapping the thickness distribution in sea ice models, J. Geophys. Res.-Oceans, 106, 13989–14000, 2001.
Lipscomb, W. H. and Hunke, E. C.: Modeling sea ice transport using incremental remapping,

Mon. Weather Rev., 132, 1341–1354, 2004.
Lunt, D. J., Haywood, A. M., Foster, G., and Stone, E. J.: The Arctic cryosphere in the mid-pliocene and the future, Phil. Trans. R. Soc. A, 367, 49–67, 2009.
Meehl, G. A., Stocker, T. F., Collins, W. D., Friedlingstein, P., Gaye, A. T., Gregory, J. M., Kitoh, A., Knutti, R., Murphy, J. M., Noda, A., Raper, S. C. B., Watterson, I. G., Weaver, A. J., and Zhao, Z. C.: Global climate projections, in: Climate Change 2007: The Physical Science Basis, Contribution of Working Group I to the Fourth Assessment Report of the Intergovernmental Panel on Climate Change, edited by: Solomon, S., Qin, D., Manning, M., Chen, Z., Marquis, M., Averyt, K. B., Tignor, M., and Miller, H. L., Cambridge University Press, Cambridge, United Kingdom and New York, NY, USA, 770–772, 2007.
Neale, R. B., Richter, J. H., Conley, A. J., Park, S., Lauritzen, P. H., Gettelman, A., Williamson, D. L., Rasch, P. J., Vavrus, S. J., Taylor, M. A., Collins, W. D., Zhang, M., and Lin, S.: Description of the NCAR Community Atmosphere Model (CAM 4.0), NCAR technical note, NCAR/TN-485+STR, 2010.
Oleson, K. W., Lawrence, D. M., Bonan, G. B., Flanner, M. G., Kluzek, E., Lawrence, P. J., Levis, S., Swenson S. C., Thornton, P., Dai, A., Decker, M., Dickinsion, R., Feddema, J., Heald, C. L., Hoffman, F., Lamarque, J., Mahowald, N., Niu, G., Qian, T., Randerson, J., Running, S., Sakaguchi, K., Slater, A., Stöckli, R., Wang, A., Yang, Z., Zeng, X., and Zeng, X.: Technical Description of version 4.0 of the Community Land Model (CLM), NCAR technical note, NCAR/TN-478+STR, 2010.
Rasch, P. J. and Kristjánsson, J. E.: A comparison of the CCM3 model climate using diagnosed and predicted condensate parameterizations, J. Climate, 11, 1587–1614, 1998.
Rasch, P. J., Mahowald, N. M., and Eaton, B. E.: Representations of transport, convection, and the hydrologic cycle in chemical transport models: Implications for the modeling of short-lived and soluble species, J. Geophys. Res., 102, 28127–28138, 1997.
Rasch, P. J., Barth, M. C., Kiehl, J. T., Schwartz, S. E., and Benkovitz, C. M.: A description of the global sulfur cycle and its controlling processes in the National Center for Atmospheric Research Community Climate Model, Version 3, J. Geophys. Res., 105, 1367–1385, 2000.
Ravelo, A. V. and Andreasen, D. H.: Enhanced circulation during a warm period, Geophys. Res. Lett., 27, 1001–1004, 2000.
Raymo, M. E., Grant, B., Horowitz, M., and Rau, G. H.: Mid-Pliocene warmth: stronger greenhouse and stronger conveyor, Mar. Micropaleontol., 27, 313–326, 1996.
Raymond, D. J. and Blyth, A. M.: A stochastic mixing model for non-precipitating cumulus

clouds, J. Atmos. Sci., 43, 2708–2718, 1986.
Raymond, D. J. and Blyth, A. M.: Extension of the stochastic mixing model to cumulonimbus clouds, J. Atmos. Sci., 49, 1968–1983, 1992.
Richter, J. H. and Rasch, P. J.: Effects of convective momentum transport on the atmospheric circulation in the community atmosphere model, version 3, J. Climate, 21, 1487–1499, 2008.
Rosenbloom, N.: Biome4 conversion to LSM, available at: https://wiki.ucar.edu/display/paleo/Biome4+conversion+to+LSM (last access: December 2011), 2009.
Rosenbloom, N., Shields, C., Brady, E., Yeager, S., and Levis, S.: CCSM3 for Paleoclimate Applications, 2010.
Rothrock, D. A.: The energetics of the plastic deformation of pack ice by ridging, J. Geophys. Res., 80, 4514–4519, 1975.
Salzmann, U., Haywood, A. M., Lunt, D. J., Valdes, P. J., and Hill, D. J.: A new global biome reconstruction and data-model comparison for the Middle Pliocene, Global Eco. Biogeogr., 17, 432–447, 2008.
Seland, Ø., Iversen, T., Kirkevåg, A., and Storelvmo, T.: Aerosol-climate interactions in the CAM-Oslo atmospheric GCM and investigation of associated basic shortcomings, Tellus, 60A, 459–491, 2008.
Simmons, A. J. and Strüfing, R.: An energy and angular-momentum conserving finite-difference scheme, hybrid coordinates and medium-range weather prediction, Technical Report ECMWF Report No. 28, European Centre for Medium-Range Weather Forecasts, Reading, UK, 68 pp., 1981.
Slingo, J. M.: The development and verification of a cloud prediction scheme for the ECMWF model, Q. J. R. Meteorol. Soc., 113, 899–927, 1987.
Sloan, L. C., Crowley, T. J., and Pollard, D.: Modeling of middle Pliocene climate with the NCAR GENESIS general circulation model, Mar. Micropaleontol., 27, 51–61, 1996.
Sohl, L. E., Chandler, M. A., Schmunk, R. B., Mankoff, Ken, Jonas, J. A., Foley, K. M., and Dowsett, H. J.: PRISM3/GISS topographic reconstruction: US Geol. Surv. Data Series, 419, 6 pp., 2009.
Thorndike, A. S., Rothrock, D. A., Maykut, G. A., and Colony, R.: The thickness distribution of sea ice, J. Geophys. Res., 80, 4501–4513, 1975.
Vertenstein, M., Craig, T., Middleton, A., Feddema, D., and Fischer, C.: CESM1.0.3 User's Guide, available at: http://www.cesm.ucar.edu/models/cesm1.0/cesm/cesm_doc/book1.html (last access: December 2011), 2010.

Yan, Q., Zhang, Z., Wang, H., Jiang, D., and Zheng, W.: Simulation of sea surface temperature changes in the Middle Pliocene warm period and comparison with reconstructions, Chinese Sci. Bull., 56, 890–899, 2011.
Zeng, X., Zhao, M., and Dickinson, R. E.: Intercomparison of bulk aerodynamic algorithms for the computation of sea surface fluxes using the TOGA COARE and TAO data, J. Climate, 11, 2628–2644, 1998.
Zhang, G. J. and McFarlane, N. A.: Sensitivity of climate simulations to the parameterization of cumulus convection in the Canadian Climate Centre general circulation model, Atmos.-Ocean, 33, 407–446, 1995.

Table 1. Boundary and initial conditions for the pre-industrial and the mid-Pliocene experiment.

Conditions	Pre-Industrial	Mid-Pliocene
Ocean model		
Landsea mask/Bathymetry	Local modern	Local modern
Initialization	Levitus T/S	Levitus T/S
Atmosphere model		
Topography	Local modern	Anomalies + local modern
CO_2	280 ppm	405 ppm
N_2O	270 ppb	270 ppb
CH_4	760 ppb	760 ppb
CFCs	0	0
Solar constant	1370 W m^{-2}	1370 W m^{-2}
Land model		
Vegetation	Local pre-industrial	PRISM vegetation
Coupler		
Orbital parameters	Year 1950	Year 1950

Table 2. Global mean value for the pre-industrial and the mid-Pliocene experiment.

Exp.	Pre-industrial	Mid-Pliocene
Top energy balance	0.04 W m^{-2}	0.13 W m^{-2}
Surface temperature	13.5 °C	16.7 °C
Precipitation	2.7 mm d^{-1}	2.9 mm d^{-1}
Sea surface temperature	17.1 °C	19.1 °C
Maximum AMOC	21.8 Sv	23.4 Sv

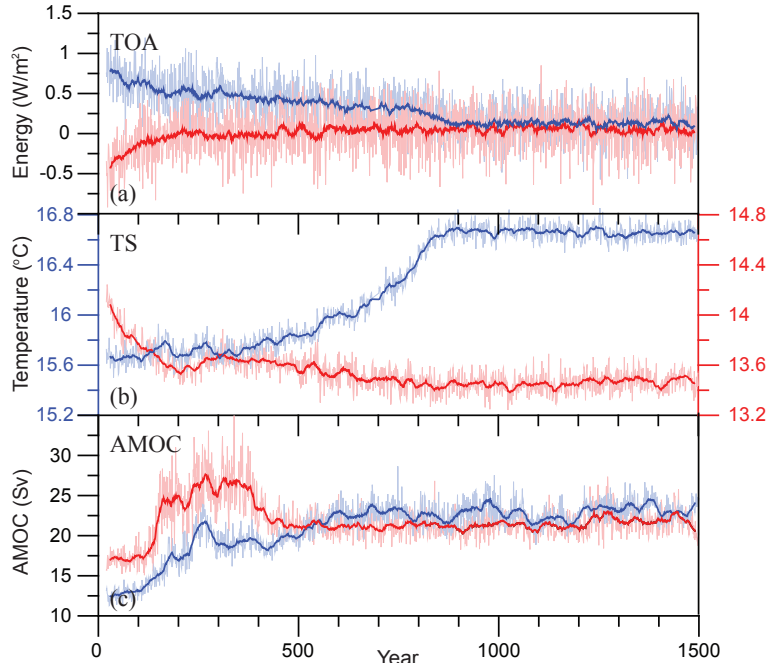

Fig. 1. Time series for **(a)** the energy balance at the top of NorESM-L ($W\,m^{-2}$), **(b)** surface temperature (°C), and **(c)** the maximum of the Atlantic overturning streamfunction (Sv) in the pre-industrial (Red) and the mid-Pliocene experiment (Blue). The thin lines show annual mean values, and the bold lines show 21-yr running averages.

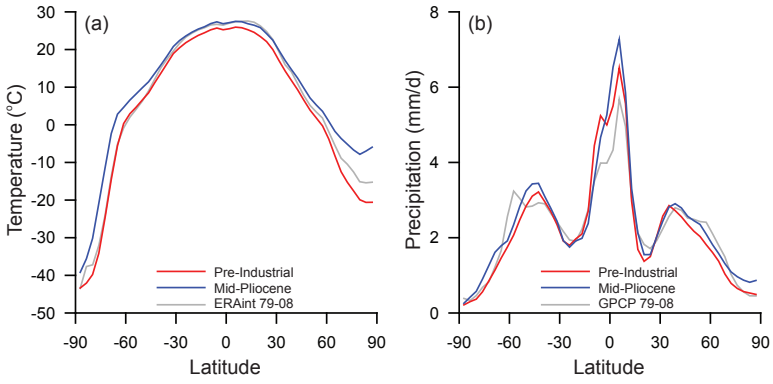

Fig. 2. Zonal mean surface temperature (**a**, °C) and precipitation (**b**, $mm\,d^{-1}$) for the observations (gray lines), the pre-industrial experiment (red lines) and the mid-Pliocene experiment (blue lines). The temperature observation is ERA-interim temperature from 1979 to 2008. The precipitation observation is the 1979–2008 precipitation from the Global Precipitation Climatology Project (GPCP).

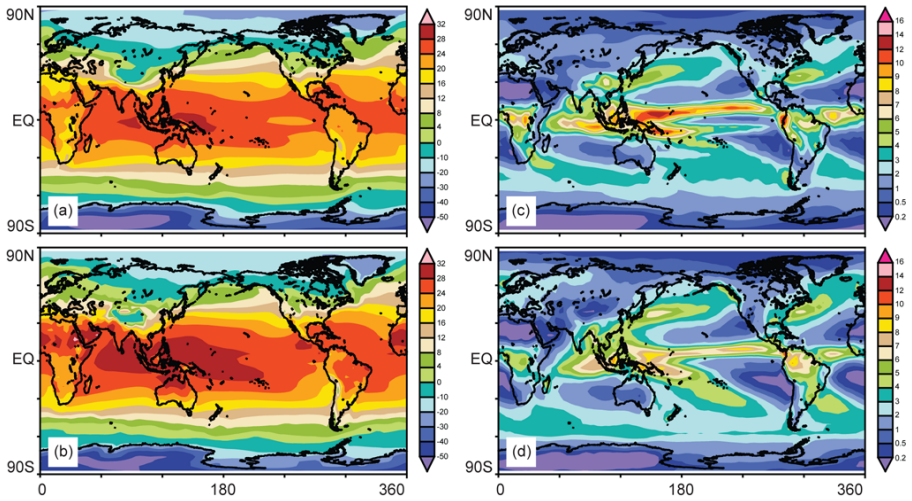

Fig. 3. Simulated annual mean pre-industrial surface temperature (**a**, °C) and precipitation (**c**, mm d^{-1}), with comparison to ERA-interim 1979–2008 surface temperature (**b**, °C) and GPCP 1979–2008 precipitation (**d**, mm d^{-1}).

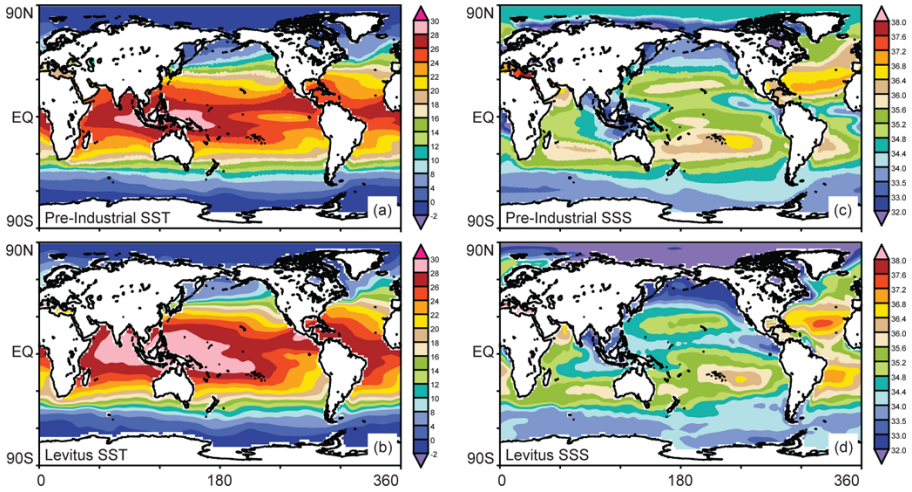

Fig. 4. Simulated annual mean pre-industrial sea surface temperature (**a**, °C) and salinity (**c**, g kg^{-1}), with comparison to LEVITUS94 sea surface temperature (**b**, °C) and salinity (**d**, psu).

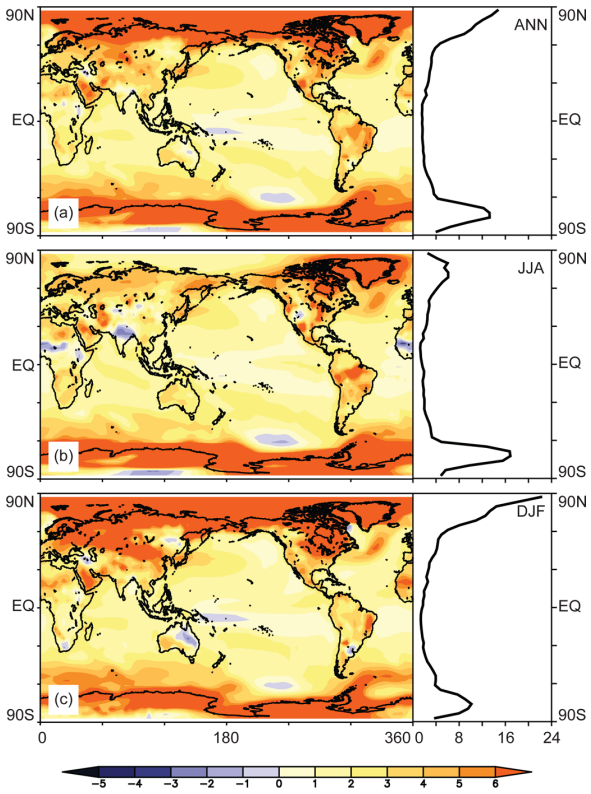

Fig. 5. Temperature differences (°C) between the mid-Pliocene and the pre-industrial experiment, **(a)** for annual mean, **(b)** for boreal summer and **(c)** for boreal winter. The bold lines on the left sides show zonal mean values.

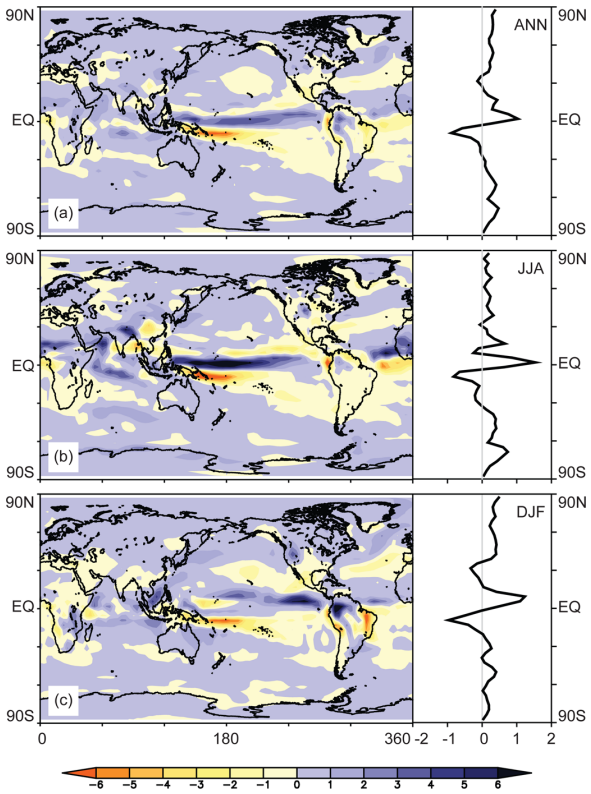

Fig. 6. Precipitation differences (mm d^{-1}) between the mid-Pliocene and the pre-industrial experiment, **(a)** for annual mean, **(b)** for boreal summer and **(c)** for boreal winter. The bold lines on the left sides show zonal mean values.

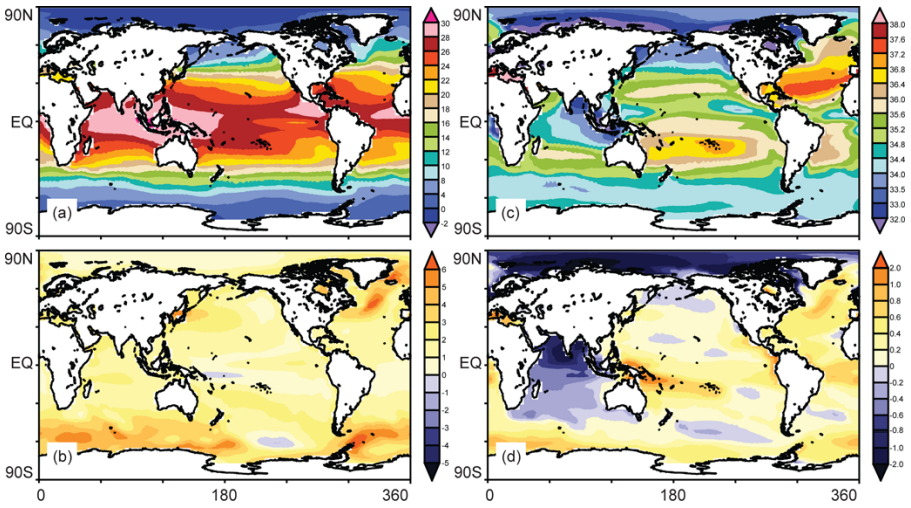

Fig. 7. Simulated mid-Pliocene SST (**a**, °C) and SSS (**c**, g kg^{-1}), and SST (**b**, °C) and SSS (**d**, g kg^{-1}) differences between the mid-Pliocene and the pre-industrial experiment.

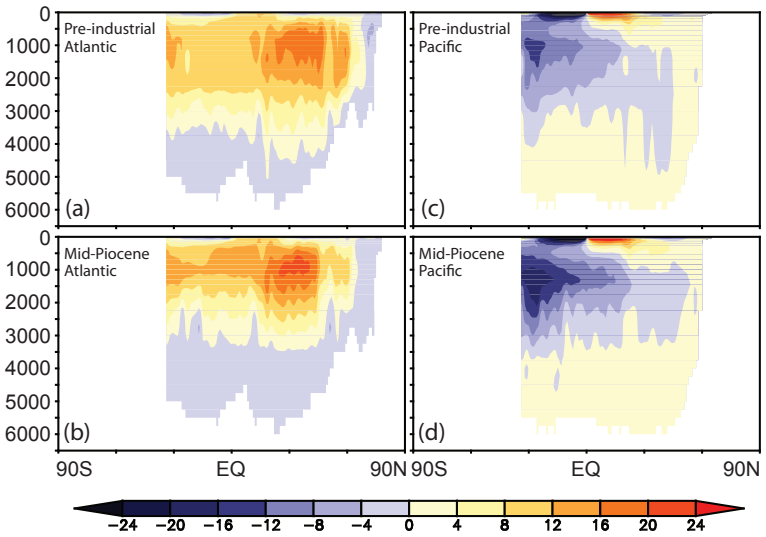

Fig. 8. Smoothed overturning streamfunction (Sv) **(a)** for pre-industrial Atlantic basin, **(b)** for mid-Pliocene Atlantic basin, **(c)** for pre-industrial Pacific basin and **(d)** for mid-Pliocene Pacific basin.